

Probing many-body effects in harmonic traps with twisted lightJ. I. Fuks^{1,2}, G. F. Quinteiro Rosen,³ H. Appel,⁴ and P. I. Tamborenea^{1,2}¹*Universidad de Buenos Aires, Facultad de Ciencias Exactas y Naturales, Departamento de Física, Buenos Aires, Argentina*²*CONICET - Universidad de Buenos Aires, Instituto de Física de Buenos Aires (IFIBA), Buenos Aires, Argentina*³*Instituto de Modelado e Innovación Tecnológica, and Departamento de Física, FaCENA, Universidad Nacional del Nordeste, 3400 Corrientes, Argentina*⁴*Max Planck Institute for the Structure and Dynamics of Matter, Luruper Chaussee 149, D-22761 Hamburg, Germany*

(Received 13 May 2021; revised 16 December 2022; accepted 3 January 2023; published 21 February 2023)

We explore the potential of twisted light, a structured beam carrying orbital angular momentum, as a tool to unveil many-body effects in parabolically confined systems. According to the generalized Kohn theorem, the dipole response of such a multiparticle system to a spatially homogeneous probe is indistinguishable from the response of a system of noninteracting particles. Twisted light however can excite internal degrees of freedom, resulting in the appearance of new peaks in the multipole spectrum which are not present when the probe is a plane wave. We also demonstrate the ability of the proposed twisted light probe to capture the transition of interacting fermions into a strongly correlated regime in a one-dimensional harmonic trap. We report that, by suitable choice of the probe's parameters, the transition into a strongly correlated phase manifests itself as an approaching and ultimate superposition of peaks in the second-order quadrupole response. These features are observed in exact calculations for two electrons and well reproduced in adiabatic time-dependent density-functional theory simulations.

DOI: [10.1103/PhysRevB.107.L081111](https://doi.org/10.1103/PhysRevB.107.L081111)**I. INTRODUCTION**

Twisted light (TL), also known as optical vortices, designates a family of highly nonhomogeneous optical beams which have single or multiple phase singularities and carry orbital angular momentum (OAM), among other interesting features [1–3]. Promising applications of TL have been identified in areas such as telecommunications [4,5], quantum computing [6], nanotechnology [7–9], and enhanced resolution imaging [10,11], to name just a few [12–14]. From a fundamental point of view, researchers seek to understand the generation, detection, and interaction of TL with matter. The latter is strongly affected by the spatial structure of the light field, and the peculiar features of TL have been shown to produce novel optical effects [14]. For example, rare transitions in atoms and nanostructures resulting from new selection rules [15–17], distinct time scales and lifetimes [18], and degree of spin polarization for OAM exchange in GaAs [19], as well as coherent photon-exciton dynamics in GaN [20] have been observed. Based on this recent progress, a variety of new phenomena undetectable by plane waves are expected to be revealed with TL. Until now there has been an emphasis on studies of the interaction of TL with single particles, to the detriment of research contemplating the role of interactions [21–24]. Here we investigate the response of multiparticle parabolically confined systems, notorious for their many-body effects going undetected when the probe is spatially homogeneous [25]. We show theoretically key ways in which the many-body physics can be unveiled by TL.

Near the ground state, electrons and holes in quantum wires and dots, ions in Paul traps, and Rydberg atoms in

optical lattices are all well described as systems of interacting particles trapped in parabolic potentials [26–29]. For atoms, the interaction is modeled as a contact potential [30], whereas for electrons and ions the interaction is via a Coulomb potential [25,31]. The correlation regime in harmonic traps can be controlled by varying the particle-particle interaction strength or the confinement ω_0 , and it also depends on the number of trapped particles.

By virtue of the high tunability and the availability of analytic (weak and strong interaction limits) [30,32,33] or very accurate one-dimensional numerical solutions [34,35], these systems provide a good testbed for many-body physics. Moreover, harmonic traps can be realized experimentally and can be used as quantum simulators to study emergent many-body phenomena such as superconductivity, superfluidity, quantum phase transitions, and topological order [36,37].

The Letter is organized as follows. In Sec. II we describe the Hamiltonian of harmonic traps containing several interacting particles and briefly review the generalized Kohn theorem. In Sec. III we present the mathematical description of twisted light and its interaction with charged particles. In Secs. IV and V we provide details on the physical system and on the computational methods, respectively. In Sec. VI we present and discuss the main results of our study and in Sec. VII we give a summary and the conclusions.

II. HARMONIC TRAP

The Hamiltonian of N particles of mass m in a harmonic trap is separable into a center of mass (c.m.) part and another part that depends on the internal degrees

of freedom, $H_0(\mathbf{r}_1 \dots \mathbf{r}_N, \mathbf{p}_1 \dots \mathbf{p}_N) = H_0^{\text{c.m.}}(\mathbf{R}, \mathbf{P}_R) + H_0^q(\mathbf{q}_1 \dots \mathbf{q}_{N-1}, \mathbf{p}_{q_1} \dots \mathbf{p}_{q_{N-1}})$; the transformation is given by the Jacobi matrix [27]. The c.m. system is equivalent to a single particle with mass $M = Nm$,

$$H_0^{\text{c.m.}} = \frac{\mathbf{P}_R^2}{2M} + \frac{1}{2}M\omega_0^2\mathbf{R}^2, \quad (1)$$

where $\mathbf{R} = (\sum_i^N \mathbf{r}_i)/N$ and $\mathbf{P}_R = \sum_i^N \mathbf{p}_i$. For $N = 2$ and taking $\mathbf{q} = (\mathbf{r}_1 - \mathbf{r}_2)/\sqrt{2}$ and $\mathbf{p}_q = (\mathbf{p}_1 - \mathbf{p}_2)/\sqrt{2}$, the internal Hamiltonian reads

$$H_0^q = \frac{\mathbf{p}_q^2}{2m} + \frac{1}{2}m\omega_0^2\mathbf{q}^2 + V_{\text{int}}(\mathbf{q}), \quad (2)$$

with $V_{\text{int}}(\mathbf{q})$ being the interaction between particles. Other definitions are valid as long as $[\mathbf{R}, \mathbf{P}_R] = i\hbar$ and $[\mathbf{q}_j, \mathbf{p}_{q_j}] = i\hbar$ hold.

The generalized Kohn theorem (GKT) [25,26] assumes a harmonic confinement of a many-electron system and the applicability of the dipole approximation to the interaction Hamiltonian between (long wavelength) light and the confined electrons. Under these two assumptions, the GKT establishes that the response is given by the center-of-mass degree of freedom or, in other words, that the electron-electron interaction does not affect the response. The same two hypotheses are made in the harmonic potential theorem [38], closely related to the GKT. The assumption of parabolic confinement holds for realistic quantum dots [27,28]. For nonharmonic traps many-body effects can be observed in the dipole spectrum [39], an effect that has been studied over the past 30 years [40–42]. Here we explore the consequences of dropping the second assumption of the GKT by studying the optical excitation of harmonically confined electrons with structured light, whose interaction cannot be modeled using the dipole approximation [43,44].

III. RESPONSE TO TWISTED LIGHT

In TL a phase singularity associated with the topological charge l gives rise to a spatially nonhomogeneous and hollow intensity distribution with vanishing electromagnetic fields at the beam center. The TL field carries OAM in the direction of propagation. We study the head-on excitation of a matter system placed at the beam center; in this case, the OAM carried by the beam is intrinsic [3]. In the Coulomb gauge, $\nabla \cdot \mathbf{A}(\mathbf{r}, t) = 0$, and the scalar potential can be chosen to vanish, $\Phi = 0$. We can then write the vector potential of a monochromatic TL field in cylindrical coordinates as [45]

$$\mathbf{A}(\mathbf{r}, t) = e^{i\theta} \left[F_{q_r, l}(r) e^{il\varphi} \mathbf{e}_\sigma - i\sigma \frac{q_r}{q_z} \frac{F_{q_r, l+\sigma}(r)}{\sqrt{2}} e^{i(l+\sigma)\varphi} \mathbf{e}_z \right] + \text{c.c.}, \quad (3)$$

with $\theta = q_z z - \omega t$ and frequency given by $\omega^2 = c^2(q_r^2 + q_z^2)$, where $1/q_r$ is a measure of the lateral beam size. The radial profile is described by a Bessel function $F_{q_r, l}(r) = A_0 J_l(q_r r)$ and the polarization vector is given by $\mathbf{e}_\sigma = e^{i\sigma\varphi}(\mathbf{e}_r + i\sigma\mathbf{e}_\varphi)/\sqrt{2} = (\mathbf{e}_x + i\sigma\mathbf{e}_y)/\sqrt{2}$. To describe the TL-matter interaction we choose the TL gauge introduced in Ref. [46]. In the TL gauge the interaction with a small, planar, and localized structure placed close to the phase singularity

TABLE I. Selection rules of one-dimensional two-particle harmonic-trap response to TL probe. Poles in brackets.

Observable	$\hat{D} = -e\hat{X}$	$\hat{Q} = -e(2\hat{X}^2 + \hat{q}^2)$
$\hat{H}_I^{l=0}$	$D_{\text{c.m.}}^{(1)} [(2n+1)\omega_0]$	$Q_{\text{c.m.}}^{(2)} [2n\omega_0]$
$\hat{H}_I^{l=1}$	$D_{\text{c.m.}}^{(2)} [(2n+1)\omega_0]$	$Q_{\text{c.m.}}^{(1)} [2n\omega_0] + Q_q^{(1)} [\omega_{02n}^q]$
$\hat{H}_I^{l=2}$	$D_{\text{c.m.}}^{(2)} [(2n+1)\omega_0]$	$Q_{\text{c.m.+q}}^{(2)} [2n\omega_0; \omega_{2n2(n+1)}^q]$

can be written in a gauge invariant form. For a parallel TL beam, $\text{sgn}(\sigma) = \text{sgn}(l)$, with circular polarization $\sigma = 1$, the interaction becomes $H_I^{\text{TL}} = [-e/(l+1)]\mathbf{r}_\perp \cdot \partial_t \mathbf{A}$, where e is the electron charge. We consider a collimated beam ($q_r/q_z \ll 1$), for which the second term in Eq. (3) can be neglected and the interaction thus simplifies to a scalar potential

$$H_I^{\text{TL}} = -\frac{ie\omega F_{q_r, l}(r)}{(l+1)} [-(x+iy)e^{i\theta} + (x-iy)e^{-i\theta}], \quad (4)$$

where we used that $x \pm iy = \mathbf{r}_\perp \cdot (\mathbf{x} \pm i\mathbf{y})$ and $r^l e^{il\varphi} = (x+iy)^l$. Near $r = 0$, we have $J_l(q_r r) \approx (q_r r)^l / (2^l l!)$. The interaction with an N -particle compact object placed at $\mathbf{r} = 0$ is then described by

$$H_I^{l=1} = \frac{eE_0 q_r}{2\sqrt{2}} \sum_{i=1}^N (x_i^2 - y_i^2) \sin(\omega t) - 2x_i y_i \cos(\omega t), \quad (5)$$

$$H_I^{l=2} = \frac{eE_0 q_r^2}{12\sqrt{2}} \sum_{i=1}^N (x_i^3 - 3x_i y_i^2) \sin(\omega t) + (y_i^3 - 3y_i x_i^2) \cos(\omega t), \quad (6)$$

where $E_0 = \omega A_0$. When $l = 0$ the field couples to the dipole.

For two particles in one dimension we can rewrite Eqs. (5) and (6) in terms of c.m. and Jacobi coordinates as

$$H_I^{l=1} = \frac{eE_0 q_r}{2\sqrt{2}} (2X^2 + q^2) \sin(\omega t), \quad (7)$$

$$H_I^{l=2} = \frac{eE_0 q_r^2}{12\sqrt{2}} (2X^3 + Xq^2) \sin(\omega t). \quad (8)$$

Notice that for $l = 1$ the interaction with TL is separable into c.m. and internal parts; for $l \geq 2$, however, separability breaks down and the system's response can no longer be described as the sum of the responses of c.m. and internal systems. For a weak applied field, the response can be expanded in a power series of the strength E_0 . The linear ($\propto E_0$) and second order ($\propto E_0^2$) responses of an observable O satisfy $\langle \hat{O}^{(1)} \rangle \propto \sum_k \langle \Psi_0 | \hat{O} | \Psi_k \rangle \langle \Psi_k | \hat{H}_I | \Psi_0 \rangle$ and $\langle \hat{O}^{(2)} \rangle \propto \sum_{k,m} \langle \Psi_0 | \hat{O} | \Psi_k \rangle \langle \Psi_k | \hat{H}_I | \Psi_m \rangle \langle \Psi_m | \hat{H}_I | \Psi_0 \rangle$ [47–50], where $\{|\Psi_k\rangle\}$ are the eigenstates of H_0 . As a consequence, only if the interaction and the observable operators have the same parity will the response be first order in the perturbation; otherwise, the first nonvanishing response will be of second order. In Table I we list the dipole ($D = \langle -e \sum_i^N \hat{x}_i \rangle$) and quadrupole ($Q = \langle -e \sum_i^N \hat{x}_i^2 \rangle$) responses of a small (compared to the beam's waist) one-dimensional harmonic trap placed at the TL probe's center (dark for $l > 0$), for three different spatial structures of the probe characterized by $l = 0, 1, 2$. The superscript labels the order of the response

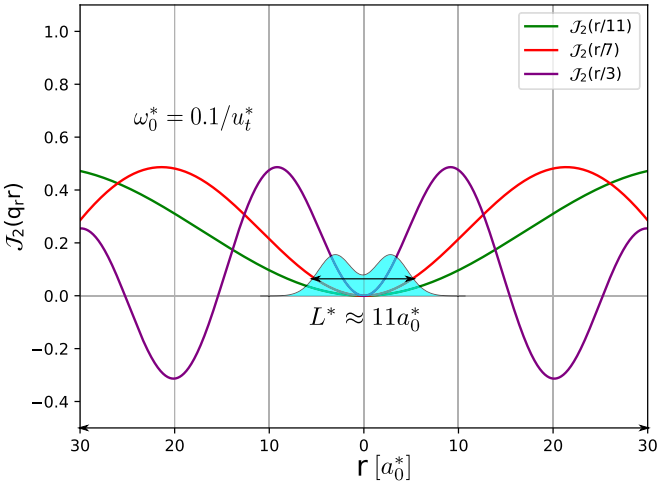


FIG. 1. Density (in cyan) of a two-electron quantum wire with confinement strength $\omega_0 = 0.1/u_t^*$ placed at the TL beam center. TL beams with $l = 2$ and lateral beam waist $1/q_r = 3a_0^*$, $7a_0^*$, and $11a_0^*$ are shown in purple, red, and green, respectively. Near $r = 0$ we can approximate $J_2(q,r) \propto (q,r)^2$ as long as $1/q_r \gg L^*$, where L^* is a measure of the system's size.

and the subscript whether the response is from the c.m., internal, or both. The frequencies of the allowed transitions are indicated in brackets. $D_{c.m.}^{(1)}[(2n+1)\omega_0]$ corresponds to GKT: for an $l = 0$ homogeneous probe the dipole response is equal to the c.m. response and first order in the field, with poles at the odd c.m. transitions $\omega_{0,(2n+1)}^{c.m.} = (2n+1)\omega_0$. We focus on the quadrupole response where the correlation effects show up (the dipole response can only reveal the c.m. spectrum; see the first column of Table I).

In order to evaluate whether a TL probe is able to capture relevant many-body physics we investigate the transition into a strongly correlated regime, which for fixed particle-particle interaction corresponds to the limit $\omega_0 \rightarrow 0$. As a proof of concept we perform numerical calculations for a system of parabolically confined electrons. We expect analogous results for multiple-ion Paul traps. The interaction between electrons is modeled with a soft-Coulomb potential [51,52]

$$V_{\text{int}}(q) = \frac{e^2}{\sqrt{(\sqrt{2}q)^2 + a^2}}. \quad (9)$$

We use atomic units (a.u.) for all the calculations, $\hbar = e = m_e = a_0 = 1$, and choose $a = 1$. In the next section we discuss realistic parameters for quantum wires and TL probes.

IV. PROBE SETUP AND SYSTEM SIZE

To ensure a large beam waist (characterized by $1/q_r$) we consider a collimated probe beam, $q_z = 2\pi/\lambda \gg q_r$. The spatial structure of the TL beam can be approximated as $J_l(q,r) \approx (q,r)^l/(2^l l!)$ near $r = 0$, which gives us control over the optical selection rules by varying l [Eqs. (5) and (6) are valid in this region]. The beam waist $1/q_r$ is to be tuned such that the system fits well within the region of validity of this approximation. In Fig. 1 we plot the spatial structure of TL beams with $l = 2$ for three different values of the beam

waist. A two-electron quantum wire is placed at the beam center and characterized by its ground state electronic density (in cyan in the figure). The maximum amplitude of the TL probe is weak, but its variation in space is strong due to the existence of the phase singularity at $r = 0$.

In order to apply the expressions to a real semiconductor use effective units of length, energy, and time defined as $a_0^* = (\epsilon/m^*)a_0$, $Ha^* = (m^*/\epsilon^2)Ha$, and $u_t^* = (\epsilon^2/m^*)u_t$, respectively, where ϵ and m^* are the relative permittivity and effective mass of the material. Taking the FWHM of the ground state electronic density as a measure of the quantum wire's length our numeric calculations for $\omega_0^* = 0.5, 0.2, 0.1$ $1/u_t^*$ yield approximate sizes of $L^* = 3, 7, 11$ a_0^* for the wires. If $\epsilon = 12.4$ and $m^* = 0.067$, which gives $a_0^* \approx 10$ nm, the lengths correspond to $L \approx 30, 70, 110$ nm, respectively.

From Fig. 1 it is evident that to probe a quantum wire of size $L^* \approx 11a_0^*$, a beam waist of $1/q_r \geq 7a_0^*$ is enough to ensure the validity of the approximation $J_2(q,r) \approx (q,r)^2/(2^2 2!)$. Within the paraxial approximation $1/q_r \geq 7a_0^*$ implies $\lambda \ll 2\pi 7a_0^* \approx 4 \times 10^{-7}$ m. A safe choice for $l = 2$ TL probe and two-electron quantum wires would be $1/q_r \geq L^*$, with $\lambda \ll 7 \times 10^{-6}$ m. A similar rationale can be applied to $l = 1$ TL beams, but notice that for $l = 1$ we have $J_1(q,r) \approx q,r/2$, which has a larger spatial derivative than the $l = 2$ case; therefore, the condition on the minimum waist size is more restrictive for $l = 1$.

We would like to stress that, since TL can be tuned with high precision in the laboratory, the requirements for the proposed setup should not be an impediment. Even less so if the proposed setup is designed as a quantum simulator, since in that case one can also tune the harmonic trap with high precision.

V. COMPUTATIONAL DETAILS

Before presenting the results of our study we discuss some relevant computational details of the calculations. Both the exact and time-dependent density-functional theory (TDDFT) dynamics were computed in OCTOPUS version 9.0 [53] using a 100 a.u. simulation box with 0.1 a.u. spacing. The exact calculations were done using the modelmb functionality in OCTOPUS [54] and the code was modified to output the quadrupole moment in one dimension.

The interaction with the TL field is modeled as $H_l^I = E_0 f(t) \sum_i x_i^{(l+1)}$ in the calculations. The spatial dependence is dictated by Eqs. (5) and (6) and for the time dependence we choose a step function $f(t) = \text{rect}(t - \tau/2)$, where τ is the duration of the pulse. For the spectra shown in the next section we used a τ equal to the time step, which is 0.005 a.u. Other choices of τ as well as a trapezoidal time function lead to qualitatively identical results in terms of the position of the peaks, which is the only feature of the spectra we analyze in this work.

The first-order quadrupole response to the TL probe can be computed as

$$Q^{(1)}(\omega) = FT[Q^{(1)}(t)]/FT[\mathcal{E}(t)], \quad (10)$$

where $\mathcal{E}(t) = E_0 f(t)$ is the external perturbation due to the interaction between the harmonic trap and the TL field. The

symmetries of the problem under study are such that whenever the interaction operator is even ($l = 0, 2$) the first-order response $Q^{(1)}$ vanishes (see Table I). In this work we focus on the first nonvanishing quadrupole response. Therefore, we analyze the first-order quadrupole response $Q^{(1)}$ in the case where the interaction operator is odd ($l = 1$) and the second-order quadrupole response $Q^{(2)}$ in the cases the interaction operator is even ($l = 0, 2$). The time-dependent quadrupole can be computed from the evolution of the density $\rho(x, t)$ as

$$Q(t) = -e \left\langle \sum_i^{N=2} \hat{x}_i^2 \right\rangle = -e \int \rho(x, t) \mathbf{x}^2 dx. \quad (11)$$

$Q^{(1)}(t)$ in Eq. (10) is simply the variation of the quadrupole moment due to the action of a TL probe of odd topological charge l , i.e., $Q^{(1)}(t) = \delta Q(t) = Q(t) - Q^0$, with $Q^0 = -e \int \rho^0(x, t) \mathbf{x}^2 dx$ being the unperturbed quadrupole moment. The second-order frequency response is not as straightforward because the hyperpolarizability is convoluted with the external field. We take a pragmatic approach in this work and approximate the second-order frequency quadrupole response as

$$Q^{(2)}(\omega) \approx FT[Q^{(2)}(t)] / (FT[\mathcal{E}(t)])^2, \quad (12)$$

where $Q^{(2)}(t) = Q(t) - Q^0$ is the variation of the quadrupole moment due to the action of a TL probe with even topological charge l . The independence of the peak positions on the shape and duration of the pulse gives us confidence that the approximation in Eq. (12) is justified. The contribution of $FT[\text{rect}(t - \tau/2)]$ is only significant around $\omega = 0$ and will be ignored here.

In addition to ALDA, we also performed calculations at the Hartree-Fock (EXX) and self-interaction corrected (SIC)-LDA level (not shown). Neither the ground state densities nor the quadrupole spectra computed using these approximations improved significantly over ALDA.

VI. RESULTS

In Fig. 2 we represent the internal potential $V(q) = 1/2m\omega_0^2 q^2 + V_{\text{int}}(q)$, the first eight eigenenergies ϵ_k^q , and first three singlet energy spacings $\omega_{mn}^q = \epsilon_m^q - \epsilon_n^q$ for confinement strengths $\omega_0 = 0.5, 0.2, 0.1$ a.u. As correlation grows we observe the emergence of several characteristic features. (i) The particles localize maximally far from each other. This is evident from the shape of $V(q)$, which transitions from a single to a double well. This behavior is also reflected in the shape of the total density (see inset Fig. 3) and is usually referred to as low density limit or Wigner crystal in the literature [55–58]. (ii) Increasing deviation of the ground state wave function from a single Slater determinant (static correlation), resulting in an increment of the von Neumann entropy s [59]: $s_{\omega_0=0.5} = 0.07$, $s_{\omega_0=0.2} = 0.25$, and $s_{\omega_0=0.1} = 0.35$. (iii) The symmetric and antisymmetric wave functions become energetically degenerate [60] as in the case of distinguishable fermions [61,62], which can be seen in the approach of even and odd internal levels (black and gray in Fig. 2) [63]. (iv) The internal energy levels become equidistant as in the case of a single-particle harmonic oscillator, with an effective natural frequency given by $\omega_{n,n+1}^q \rightarrow \sqrt{3} \omega_0/2$ as $\omega_0 \rightarrow 0$, consistent with a Taylor expansion of the Coulomb potential around

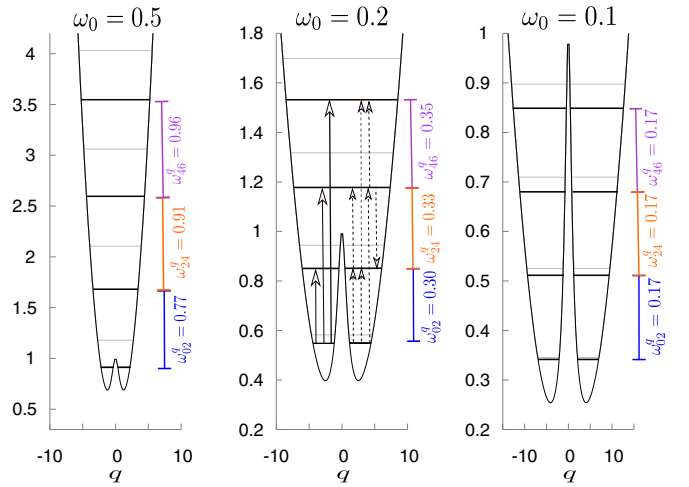


FIG. 2. Internal potential $V(q)$, eigenvalues ϵ_n^q , and the singlet energy spacings $\omega_{mn}^q = \epsilon_m^q - \epsilon_n^q$ in the low energy region (atomic units). Energy levels in black (gray) represent singlet (triplet) states. The solid (dashed) arrows represent the first order $Q_q^{(1)}$ (second order $Q_q^{(2)}$) quadrupole response to a quadrupole excitation.

the classical equilibrium positions of the particles [32,64]. We show that, of all these features, the equidistance between quadrupole response frequencies [feature (iv)] can be identified by means of a TL probe.

The arrows in Fig. 2 represent the quadrupole-allowed internal transitions in the low-energy region. Solid arrows connect the ground state with even states and represent the first-order quadrupole response $Q_q^{(1)}$; these transitions can be excited with a TL probe of $l = 1$. Dashed arrows correspond to $Q_q^{(2)}$ which depends on two frequencies (two-photon processes). These transitions connect even internal states and can be excited with an $l = 2$ TL probe (see Table I).

We envisage a large waist TL beam impinging head-on at an object placed near the beam center, such that $q_r r \ll 1$ and $J_l(q_r r) \approx (q_r r)^l / (2^l l!)$ (see Fig. 1), which gives us control over the optical allowed excitations by varying l . The interaction with the TL probe is modeled as a weak instant field, $H_l^I = E_0 \sum_i^N r_i^{(l+1)} \text{rect}(t - 0.0025 \text{ a.u.})$.

In Fig. 3 we plot the quadrupole spectra of two-electron harmonic traps, for different regimes of confinement ω_0 . The exact response is shown in black and in green we show the TDDFT response computed using the adiabatic local-density approximation (ALDA), for TL probes of $l = 0, 1, 2$. To analyze the peak positions we plot the absolute value of the Fourier transform (FT) of the quadrupole, $Q(\omega) = |FT[-e \int \rho(x, t) \mathbf{x}^2 dx]|$, computed from real-time evolution of the electronic density $\rho(x, t)$. After the perturbation is turned off the system evolves freely for a total time of $T = 2500$ a.u. TL-matter interaction in the problem under study is modeled as a scalar potential and can therefore be fully characterized by density-density response. The imaginary parts of $Q^{(1)}(\omega)$ and $Q^{(2)}(\omega)$ correspond to the quadrupole polarizability and first quadrupole hyperpolarizability, respectively [65,66], which can be measured in an absorption experiment [67,68].

Interaction with a homogeneous probe $l = 0$ shown in the upper panel of Fig. 3 gives the c.m. quadrupole response

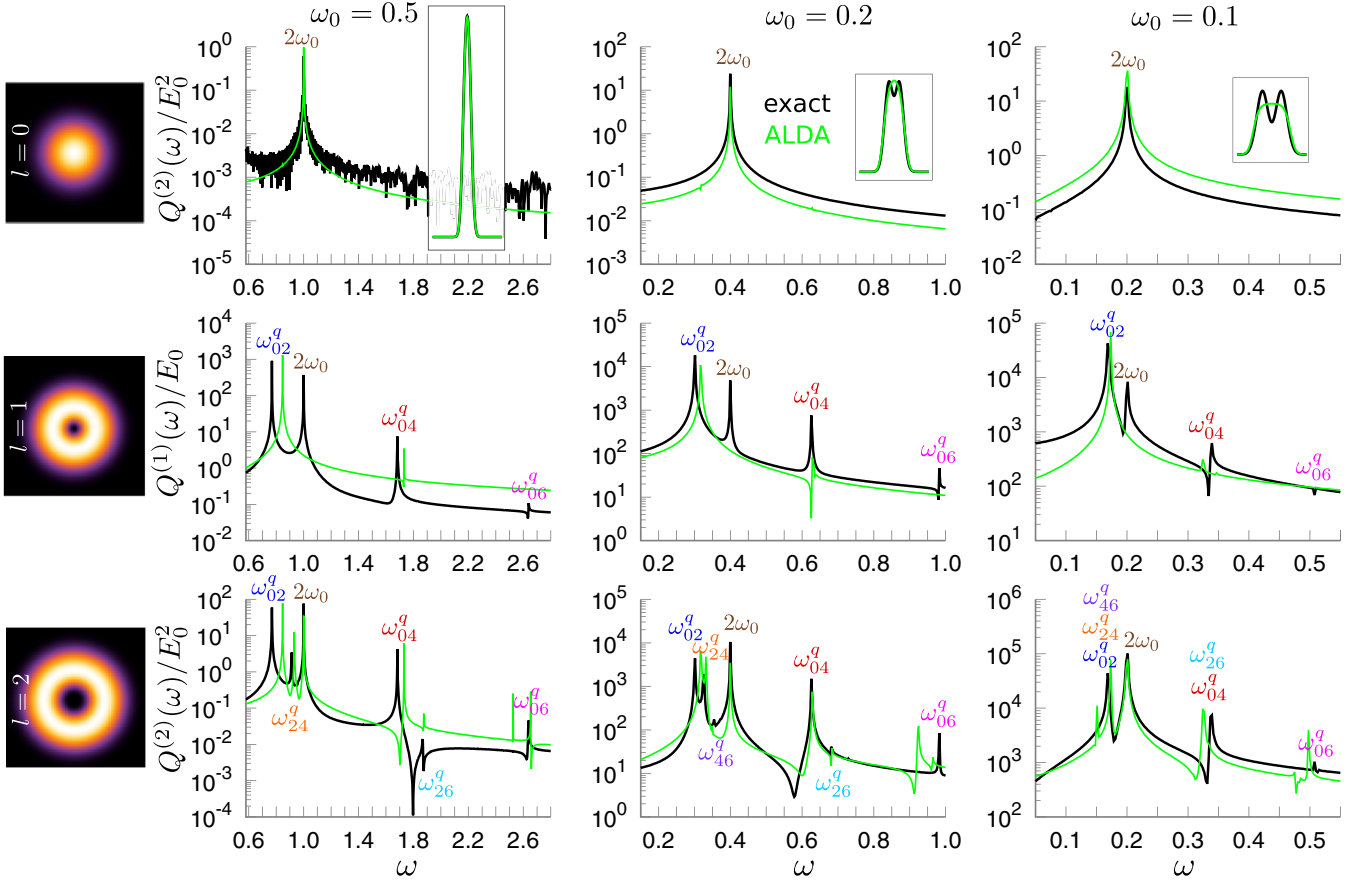


FIG. 3. Exact (black) and ALDA (green) quadrupole spectrum (in log scale) of a two-electron one-dimensional harmonic trap excited with a homogeneous $l = 0$ probe (upper panel), a $l = 1$ TL probe (middle panel), and a $l = 2$ TL probe (lower panel). The object is placed at the beam center (dark for $l > 0$). The ground state densities are shown in the inset. Numerical values for ω_{mn}^q in Fig. 2 (atomic units). See computational details in the text.

$Q_{\text{c.m.}}^{(2)}[2\omega_0]$. ALDA reproduces the position of the peak accurately. For the $l = 1$ TL probe shown in the middle panel the quadrupole response is $Q_{\text{c.m.}}^{(1)}[2\omega_0] + Q_q^{(1)}[\omega_{02}^q, \omega_{04}^q, \omega_{06}^q]$. The four internal transitions and their numerical values are indicated with solid arrows in Fig. 2. As correlation grows ($\omega_0 \rightarrow 0$) the singlet internal transitions become equidistant and independent of the interaction, $\omega_{2n,2(n+1)}^q \rightarrow \sqrt{3}\omega_0$. ALDA shows one unique peak instead of two for $l = 1$; this shortcoming is well understood [69] and can be fixed *ad hoc* as shown in Ref. [70], where accurate energies for the transitions ω_{02}^q and $\omega_{02}^{\text{c.m.}}$ were found for the same one-dimensional Hooke's atom studied here. For the $l = 2$ TL probe shown in the lower panel the quadrupole response is $Q_{\text{c.m.+q}}^{(2)}[\omega_{02}^q, 2\omega_0, \omega_{04}^q, \omega_{06}^q, \omega_{24}^q, \omega_{46}^q, \omega_{26}^q]$; the transitions are indicated with dashed arrows in Fig. 2. As we move into the strongly correlated regime the transition frequencies $\omega_{02}^q, \omega_{24}^q$, and ω_{46}^q get closer and so do ω_{04}^q and ω_{26}^q . For $\omega_0 = 0.1$ a.u. they overlap at the theoretical value $\omega_{2n,2(n+1)}^q \rightarrow \sqrt{3}\omega_0$ and $\omega_{2n,2(n+2)}^q \rightarrow 2\sqrt{3}\omega_0$, respectively, as predicted theoretically for the limit $\omega_0 \rightarrow 0$ [32,33]. ALDA reproduces the position of the peaks fairly well in the $l = 2$ spectra for all ω_0 , capturing the approaching and overlapping of the peaks as the confinement ω_0 decreases and correlation dominates. Despite reproducing poorly the ground state density in this limit [57]

(see inset Fig. 3) ALDA's spectrum seems to get actually more accurate for small ω_0 . We may speculate that the equidistant spacing of the internal energy levels is easier for the TDDFT approximation to capture because it renders the response effectively single particle.

For $\omega_0 = 0.1$ and an $l = 2$ TL probe we observe an additional peak in the low energy region (≈ 0.15 a.u.) of the ALDA spectrum (see lowest energy peak in green spectrum in Fig. 3). The emergence of this spurious peak coincides with the appearance of a degeneracy between two ALDA frequencies, namely $\omega_{06}^{q,\text{ALDA}} - \omega_{04}^{q,\text{ALDA}} = \omega_{02}^{q,\text{ALDA}} \approx 0.17$ a.u. We only observe the spurious peak when such a degeneracy takes place (both in ALDA and in Hartree-Fock). We hypothesize that this unphysical peak could be related to the spurious poles plaguing adiabatic TDDFT and Hartree-Fock quadrupole response in cases of degeneracy between TDDFT frequencies [71], but further investigation is needed to confirm this hypothesis.

VII. CONCLUSION

We have shown analytically that, unlike plane waves, a TL field is able to excite internal transitions in harmonically confined systems of interacting particles. We identify several features that characterize the transition into a strongly

correlated regime in a many-particle harmonic trap. Out of them the degeneracy between symmetric and antisymmetric wave functions has been experimentally observed in nanowires and in a one-dimensional atom trap [55,72]. We show that another characteristic feature, namely the equidistance between internal energy levels, can be revealed in the quadrupole response after excitation with a TL probe. We present the numerically exact response of a two-electron quantum wire perturbed with a TL probe of $l = 0, 1, 2$ and show that the results can be reproduced with an *ab initio* method such as adiabatic TDDFT. The validity of our findings is expected to hold for an arbitrary number of particles, as supported by our preliminary ALDA simulations for three electrons (not shown in this Letter). We expect that, in the case of a two-dimensional harmonic trap, the quadrupole response contains information on the moment of inertia; this may prove useful to study angular momentum exchange [73] or superfluidity [74].

We conclude that a TL probe can be used for noninvasive internal state detection and to study correlation effects and novel optical selection rules in harmonic traps like quantum

dots or ion traps. If the TL probe is replaced by a resonant TL pump it could also be used to control the internal state of the quantum system. Manipulation and detection of the internal (motional) modes is key for the implementation of logical gates in ion-trap quantum computing [29,75,76]. The proposed setup could serve as an analog quantum simulator to control and study intermediate correlation regimes where no analytic or numerically accurate solutions are available. Alternatively it could also be used to characterize the TL field. Whether a TL probe can provide additional information about the degree of correlation in the more general case of nonharmonic systems for which GKT does not apply remains as an open question.

ACKNOWLEDGMENTS

J.I.F. and P.I.T. gratefully acknowledge the financial support from the Universidad de Buenos Aires, Project UBACyT 2018 Grant No. 20020170100711BA. G.F.Q.R. thanks ONRG for support through Grant No. N62909-18-1-2090.

-
- [1] L. Allen, S. Barnett, and M. Padgett, *Optical Angular Momentum*, Food Science & Technology (Taylor & Francis, London, 2003).
- [2] D. Andrews, *Structured Light and Its Applications: An Introduction to Phase-Structured Beams and Nanoscale Optical Forces* (Elsevier Science, Amsterdam, 2011).
- [3] K. Y. Bliokh and F. Nori, Transverse and longitudinal angular momenta of light, *Phys. Rep.* **592**, 1 (2015).
- [4] M. P. Lavery, C. Peuntinger, K. Günthner, P. Banzer, D. Elser, R. W. Boyd, M. J. Padgett, C. Marquardt, and G. Leuchs, Free-space propagation of high-dimensional structured optical fields in an urban environment, *Sci. Adv.* **3**, e1700552 (2017).
- [5] A. E. Willner, Twisted Light Could Dramatically Boost Data Rates, *IEEE Spectrum* (IEEE, Piscataway, NJ, 2016), <https://spectrum.ieee.org/twisted-light-could-dramatically-boost-data-rates>.
- [6] M. Erhard, R. Fickler, M. Krenn, and A. Zeilinger, Twisted photons: new quantum perspectives in high dimensions, *Light Sci. Appl.* **7**, 17146 (2018).
- [7] X. Cai, J. Wang, M. J. Strain, B. Johnson-Morris, J. Zhu, M. Sorel, J. L. O'Brien, M. G. Thompson, and S. Yu, Integrated compact optical vortex beam emitters, *Science* **338**, 363 (2012).
- [8] D. Schulze, A. Thakur, A. S. Moskalenko, and J. Berakdar, Accelerating, guiding, and sub-wavelength trapping of neutral atoms with tailored optical vortices, *Ann. Phys. (NY)* **529**, 1600379 (2017).
- [9] Y. Chen, J. Gao, Z.-Q. Jiao, K. Sun, W.-G. Shen, L.-F. Qiao, H. Tang, X.-F. Lin, and X.-M. Jin, Mapping Twisted Light Into and Out of a Photonic Chip, *Phys. Rev. Lett.* **121**, 233602 (2018).
- [10] M. Ritsch-Martel, Orbital angular momentum light in microscopy, *Philos. Trans. R. Soc. A* **375**, 20150437 (2017).
- [11] L. Thibon, L. E. Lorenzo, M. Piché, and Y. De Koninck, Resolution enhancement in confocal microscopy using Bessel-Gauss beams, *Opt. Express* **25**, 2162 (2017).
- [12] A. Mann, Twisted light beams promise an optical revolution, *Proc. Natl. Acad. Sci. USA* **115**, 5621 (2018).
- [13] Y. Shen, X. Wang, Z. Xie, C. Min, X. Fu, Q. Liu, M. Gong, and X. Yuan, Optical vortices 30 years on: OAM manipulation from topological charge to multiple singularities, *Light Sci. Appl.* **8**, 90 (2019).
- [14] G. F. Quinteiro Rosen, P. I. Tamborenea, and T. Kuhn, Interplay between optical vortices and condensed matter, *Rev. Mod. Phys.* **94**, 035003 (2022).
- [15] C. T. Schmiegelow, J. Schulz, H. Kaufmann, T. Ruster, U. G. Poschinger, and F. Schmidt-Kaler, Transfer of optical orbital angular momentum to a bound electron, *Nat. Commun.* **7**, 12998 (2016).
- [16] A. Afanasev, C. E. Carlson, C. T. Schmiegelow, J. Schulz, F. Schmidt-Kaler, and M. Solyanik, Experimental verification of position-dependent angular-momentum selection rules for absorption of twisted light by a bound electron, *New J. Phys.* **20**, 023032 (2018).
- [17] S. Reich, N. S. Mueller, and M. Bubula, Selection rules for structured light in nanooligomers and other nanosystems, *ACS Photon.* **7**, 1537 (2020).
- [18] M. A. Noyan and J. M. Kikkawa, Time-resolved orbital angular momentum spectroscopy, *Appl. Phys. Lett.* **107**, 032406 (2015).
- [19] L. A. Sordillo, S. Mamani, M. Sharonov, and R. R. Alfano, The interaction of twisted Laguerre-Gaussian light with a GaAs photocathode to investigate photogenerated polarized electrons, *Appl. Phys. Lett.* **114**, 041104 (2019).
- [20] K. Shigematsu, Y. Toda, K. Yamane, and R. Morita, Orbital angular momentum spectral dynamics of GaN excitons excited by optical vortices, *Jpn. J. Appl. Phys.* **52**, 08JL08 (2013).
- [21] G. F. Quinteiro, Below-bandgap excitation of bulk semiconductors by twisted light, *Europhys. Lett.* **91**, 27002 (2010).
- [22] M. Babiker, D. L. Andrews, and V. E. Lembessis, Atoms in complex twisted light, *J. Opt.* **21**, 013001 (2019).
- [23] M. Holtkemper, D. E. Reiter, and T. Kuhn, Influence of the quantum dot geometry on p-shell transitions in differently charged quantum dots, *Phys. Rev. B* **97**, 075308 (2018).
- [24] J. Wätzel, J. Berakdar, and E. Y. Sherman, Ultrafast entanglement switching and singlet-triplet transitions control

- via structured terahertz pulses, *New J. Phys.* **24**, 043016 (2022).
- [25] L. Brey, N. F. Johnson, and B. I. Halperin, Optical and magneto-optical absorption in parabolic quantum wells, *Phys. Rev. B* **40**, 10647 (1989).
- [26] S. Yip, Magneto-optical absorption by electrons in the presence of parabolic confinement potentials, *Phys. Rev. B* **43**, 1707 (1991).
- [27] L. Jacak, P. Hawrylak, and A. Wojs, *Quantum Dots* (Springer Science & Business Media, New York, 2013).
- [28] H. A. Sarkisyan, D. B. Hayrapetyan, L. S. Petrosyan, E. M. Kazaryan, A. N. Sofronov, R. M. Balagula, D. A. Firsov, L. E. Vorobjev, and A. A. Tonkikh, Realization of the Kohn's theorem in Ge/Si quantum dots with hole gas: Theory and experiment, *Nanomaterials* **9**, 56 (2019).
- [29] R. Blatt and D. Wineland, Entangled states of trapped atomic ions, *Nature (London)* **453**, 1008 (2008).
- [30] T. Busch, B.-G. Englert, K. Rzazewski, and M. Wilkens, Two cold atoms in a harmonic trap, *Found. Phys.* **28**, 549 (1998).
- [31] X.-L. Deng, D. Porras, and J. I. Cirac, Quantum phases of interacting phonons in ion traps, *Phys. Rev. A* **77**, 033403 (2008).
- [32] M. Taut, Two electrons in an external oscillator potential: Particular analytic solutions of a Coulomb correlation problem, *Phys. Rev. A* **48**, 3561 (1993).
- [33] M. Taut, K. Pernal, J. Cioslowski, and V. Staemmler, Three electrons in a harmonic oscillator potential: Pairs versus single particles, *J. Chem. Phys.* **118**, 4861 (2003).
- [34] S. E. Gharashi and D. Blume, Correlations of the Upper Branch of 1D Harmonically Trapped Two-Component Fermi Gases, *Phys. Rev. Lett.* **111**, 045302 (2013).
- [35] T. Grining, M. Tomza, M. Lesiuk, M. Przybytek, M. Musiał, P. Massignan, M. Lewenstein, and R. Moszynski, Many interacting fermions in a one-dimensional harmonic trap: A quantum-chemical treatment, *New J. Phys.* **17**, 115001 (2015).
- [36] I. M. Georgescu, S. Ashhab, and F. Nori, Quantum simulation, *Rev. Mod. Phys.* **86**, 153 (2014).
- [37] L. Tarruell and L. Sanchez-Palencia, Quantum simulation of the hubbard model with ultracold fermions in optical lattices, *C. R. Phys.* **19**, 365 (2018).
- [38] J. F. Dobson, Harmonic-Potential Theorem: Implications for Approximate Many-Body Theories, *Phys. Rev. Lett.* **73**, 2244 (1994).
- [39] A. Ballester, J. Movilla, J. Escartín, M. Pi, and J. Pannelles, Configuration interaction approach to fermi liquid-wigner crystal mixed phases in semiconductor nanodumbbells, *J. Appl. Phys.* **112**, 024311 (2012).
- [40] K. Karraï, X. Ying, H. D. Drew, M. Santos, M. Shayegan, S. R. E. Yang, and A. H. MacDonald, Magnetorotons in Quasi-Three-Dimensional Electron Systems, *Phys. Rev. Lett.* **67**, 3428 (1991).
- [41] X. Ying, K. Karraï, H. D. Drew, M. Santos, and M. Shayegan, Collective cyclotron resonance of an inhomogeneous electron gas, *Phys. Rev. B* **46**, 1823 (1992).
- [42] P. I. Tamborenea and S. Das Sarma, Collective excitations in imperfect parabolic quantum wells with in-plane magnetic fields, *Phys. Rev. B* **49**, 16593 (1994).
- [43] S. A. Mikhailov, Response of a system of strongly interacting particles to an inhomogeneous external field, *Phys. Lett. A* **240**, 354 (1998).
- [44] M. Wagner, A. V. Chaplik, and U. Merkt, Quadrupole excitations of quantum dots, *Phys. Rev. B* **51**, 13817 (1995).
- [45] G. F. Quinteiro, C. T. Schmiegelow, D. E. Reiter, and T. Kuhn, Reexamination of Bessel beams: A generalized scheme to derive optical vortices, *Phys. Rev. A* **99**, 023845 (2019).
- [46] G. F. Quinteiro, D. E. Reiter, and T. Kuhn, Formulation of the twisted-light-matter interaction at the phase singularity: The twisted-light gauge, *Phys. Rev. A* **91**, 033808 (2015).
- [47] A. L. Fetter and J. D. Walecka, *Quantum Theory of Many-Particle Systems* (Courier Corporation, North Chelmsford, MA, 2012).
- [48] G. Giuliani and G. Vignale, *Quantum Theory of the Electron Liquid* (Cambridge University Press, Cambridge, UK, 2005).
- [49] J.-I. Iwata, K. Yabana, and G. Bertsch, Real-space computation of dynamic hyperpolarizabilities, *J. Chem. Phys.* **115**, 8773 (2001).
- [50] C. Gray and B. Lo, Spherical tensor theory of molecular multipole moments and polarizabilities, *Chem. Phys.* **14**, 73 (1976).
- [51] R. Loudon, One-dimensional hydrogen atom, *Proc. R. Soc. A* **472**, 20150534 (2016).
- [52] F. Grasselli, Variational approach to the soft-coulomb potential in low-dimensional quantum systems, *Am. J. Phys.* **85**, 834 (2017).
- [53] N. Tancogne-Dejean, M. J. Oliveira, X. Andrade, H. Appel, C. H. Borca, G. Le Breton, F. Buchholz, A. Castro, S. Corni, A. A. Correa *et al.*, Octopus, a computational framework for exploring light-driven phenomena and quantum dynamics in extended and finite systems, *J. Chem. Phys.* **152**, 124119 (2020).
- [54] N. Helbig, J. I. Fuks, I. Tokatly, H. Appel, E. Gross, and A. Rubio, Time-dependent density-functional and reduced density-matrix methods for few electrons: Exact versus adiabatic approximations, *Chem. Phys.* **391**, 1 (2011).
- [55] S. Pecker, F. Kuemmeth, A. Secchi, M. Rontani, D. Ralph, P. McEuen, and S. Ilani, Observation and spectroscopy of a two-electron wigner molecule in an ultraclean carbon nanotube, *Nat. Phys.* **9**, 576 (2013).
- [56] D. D. Vu and S. Das Sarma, One-dimensional few-electron effective Wigner crystal in quantum and classical regimes, *Phys. Rev. B* **101**, 125113 (2020).
- [57] F. Malet and P. Gori-Giorgi, Strong Correlation in Kohn-Sham Density Functional Theory, *Phys. Rev. Lett.* **109**, 246402 (2012).
- [58] E. Räsänen, H. Saarikoski, M. J. Puska, and R. M. Nieminen, Wigner molecules in polygonal quantum dots: A density-functional study, *Phys. Rev. B* **67**, 035326 (2003).
- [59] P. Ziesche, Correlation strength and information entropy, *Int. J. Quantum Chem.* **56**, 363 (1995).
- [60] L. Guan, S. Chen, Y. Wang, and Z.-Q. Ma, Exact Solution for Infinitely Strongly Interacting Fermi Gases in Tight Waveguides, *Phys. Rev. Lett.* **102**, 160402 (2009).
- [61] E. Cuestas, M. D. Jiménez, and A. P. Majtey, Entanglement and fermionization of two distinguishable fermions in a strict and non strict one-dimensional space, *J. Phys. A: Math. Theor.* **54**, 025302 (2021).
- [62] T. Sowiński, T. Grass, O. Dutta, and M. Lewenstein, Few interacting fermions in a one-dimensional harmonic trap, *Phys. Rev. A* **88**, 033607 (2013).
- [63] For separable systems it is the parity of the internal wave function that determines the particle exchange symmetry and thus also the symmetry of the spin wave function. See

- L. D. Landau and E. M. Lifshitz, *Quantum Mechanics: Non-relativistic Theory*, Vol. 3 (Elsevier, Amsterdam, 2013).
- [64] J. H. Jefferson and W. Häusler, Effective charge-spin models for quantum dots, *Phys. Rev. B* **54**, 4936 (1996).
- [65] A. D. Buckingham, Polarizability and hyperpolarizability, *Philos. Trans. R. Soc. London A* **293**, 239 (1979).
- [66] G. Higgins, C. Zhang, F. Pokorny, H. Parke, E. Jansson, S. Salim, and M. Hennrich, Observation of second- and higher-order electric quadrupole interactions with an atomic ion, *Phys. Rev. Res.* **3**, L032032 (2021).
- [67] S. Tojo, M. Hasuo, and T. Fujimoto, Absorption Enhancement of an Electric Quadrupole Transition of Cesium Atoms in an Evanescent Field, *Phys. Rev. Lett.* **92**, 053001 (2004).
- [68] T. Ray, R. K. Gupta, V. Gokhroo, J. L. Everett, T. Nieddu, K. S. Rajasree, and S. N. Chormaic, Observation of the $87\text{rb } 5s_{1/2}$ to $4d_{3/2}$ electric quadrupole transition at 516.6 nm mediated via an optical nanofibre, *New J. Phys.* **22**, 062001 (2020).
- [69] M. A. Marques, N. T. Maitra, F. M. Nogueira, E. K. Gross, and A. Rubio, *Fundamentals of Time-Dependent Density Functional Theory* (Springer, Berlin, 2012), Vol. 837.
- [70] N. T. Maitra, F. Zhang, R. J. Cave, and K. Burke, Double excitations within time-dependent density functional theory linear response, *J. Chem. Phys.* **120**, 5932 (2004).
- [71] S. M. Parker, S. Roy, and F. Furche, Unphysical divergences in response theory, *J. Chem. Phys.* **145**, 134105 (2016).
- [72] G. Zürn, F. Serwane, T. Lompe, A. N. Wenz, M. G. Ries, J. E. Bohn, and S. Jochim, Fermionization of Two Distinguishable Fermions, *Phys. Rev. Lett.* **108**, 075303 (2012).
- [73] M. Babiker, C. R. Bennett, D. L. Andrews, and L. D. Dávila Romero, Orbital Angular Momentum Exchange in the Interaction of Twisted Light with Molecules, *Phys. Rev. Lett.* **89**, 143601 (2002).
- [74] F. Zambelli and S. Stringari, Moment of inertia and quadrupole response function of a trapped superfluid, *Phys. Rev. A* **63**, 033602 (2001).
- [75] K. R. Brown, J. Chiaverini, J. M. Sage, and H. Häffner, Materials challenges for trapped-ion quantum computers, *Nat. Rev. Mater.* **6**, 892 (2021).
- [76] M. Oral, O. Číp, and L. Slodička, Simulation of motion of many ions in a linear Paul trap, *Int. J. Mod. Phys. A* **34**, 1942003 (2019).